An L_1-based variational model for Retinex theory and its application to medical images

Wenye Ma[1], Jean-Michel Morel[2], Stanley Osher[1], Aichi Chien[3]
[1]Department of Mathematics, University of California, Los Angeles, CA, USA
[2]CMLA, ENS Cachan, Paris, France
[3]Department of Radiological Sciences, University of California, Los Angeles, CA, USA
mawenye@math.ucla.edu, morel@cmla.ens-cachan.fr, sjo@math.ucla.edu, aichi@ucla.edu

Abstract

Human visual system (HVS) can perceive constant color under varying illumination conditions while digital images record information of both reflectance (physical color) of objects and illumination. Retinex theory, formulated by Edwin H. Land, aimed to simulate and explain this feature of HVS. However, to recover the reflectance from a given image is in general an ill-posed problem. In this paper, we establish an L_1-based variational model for Retinex theory that can be solved by a fast computational approach based on Bregman iteration. Compared with previous works, our L_1-Retinex method is more accurate for recovering the reflectance, which is illustrated by examples and statistics. In medical images such as magnetic resonance imaging (MRI), intensity inhomogeneity is often encountered due to bias fields. This is a similar formulation to Retinex theory while the MRI has some specific properties. We then modify the L_1-Retinex method and develop a new algorithm for MRI data. We demonstrate the performance of our method by comparison with previous work on simulated and real data.

1. Introduction

Digital images are sometimes different from the scene directly perceived by the human visual system (HVS). Our visual system can automatically discount the variation of the illumination which ensures that the perceived color remains constant under varying illumination conditions. This feature is called color constancy. Edwin H. Land's Retinex theory [1, 2, 3, 4] is the first computational model that aims to simulate the HVS. The basic assumptions of Retinex theory are

(i). The HVS performs the same computation in each of three independent color channels (RGB);

(ii). In each color channel, the image intensity is proportional to the product of the reflectance of objects and the illumination;

(iii). The reflectance of object can be perceived by HVS while the illumination is automatically discounted.

Moreover, it is assumed that the reflectance is the sharp detail in the image (*i.e.* edges) and thus piecewise constant whereas the illumination is spatially smooth. The primary goal of Retinex theory is to decompose a given image I into to two different images, the reflectance R and the illumination E such that

$$I(\mathbf{x}) = R(\mathbf{x})E(\mathbf{x}) \qquad (1)$$

at each pixel $\mathbf{x}$.
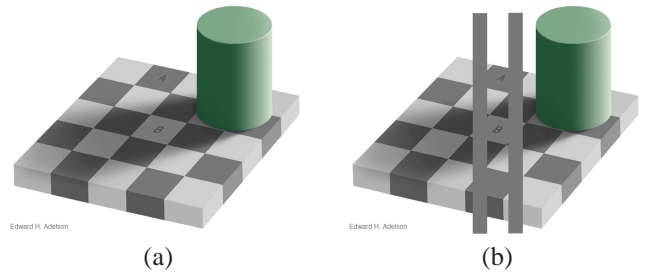
Figure 1. Adelson's checker shadow illusion. (a): Original image. (b): Demonstration.

For example, in Figure-1, the image is called "Adelson's checker shadow illusion". For us, the region A seems darker than the region B, but they actually have exactly the same color. This is because, by Retinex theory, they are in different illumination conditions. Actually, the region B is in the shadow of the green cylinder so that the illumination of the region A is stronger than that of the region B, *i.e.*, $E(A) > E(B)$. By Retinex theory, the reflectance of the region A is smaller than that of the region B, *i.e.*,

$R(A) < R(B)$ to ensure $I(A) = I(A)$. For a human being, the illumination E is discounted by the HVS and only the reflectance R is perceived, which is the reason why the region A seems darker.

To simulate the mechanism of HVS, we need to recover the reflectance R from a given image I, which is in general an ill-posed problem. To overcome this problem, many algorithms were developed. Retinex algorithms are basically categorized [8, 9, 10, 11] as path-based algorithms, recursive algorithms, center/surround algorithms, PDE-based algorithms, and variational algorithms. Path-based algorithms [1, 3, 12] consider the reflectance at each pixel depending on the multiplication of the ratios along random walks and then stochastic theory is applied. Path-based algorithms need a large number of parameters and have high computation complexity. Recursive algorithms [14, 15] extend the path-based algorithms and replace the path computation by a recursive matrix calculation which highly improves the computational efficiency. But the number of iterations is not clearly defined and can strongly influence the final result. The center/surround approaches [1, 17] such as SSR (Single Scale Retinex) and MSR (Multiscale Retinex) are based on the idea that the illumination component tends to change smoothly, contrarily to the reflectance. So the output reflectance values can be computed by subtracting a blurred version of the input image. These algorithms are easy to implement but need too many parameters. In the PDE-based formulations [5, 6, 7, 8], threshold functions are usually utilized to eliminate the illumination. Then the reflectance can be recovered by solving Poisson equations which can be done by effective algorithms such as FFT. However, extra nonsparse divergence free vector fields are introduced to the gradient when we solve the Poisson equations and thus the recovered reflectance is usually not piecewise constant as expected. Variational methods [9, 10] introduce regularization on reflectance and illumination based on the properties of them. Some regularization terms such as total variation (TV) are introduced to ensure getting piecewise constant reflectance. But they eliminate too much information. Therefore, in this paper, we develop a new L_1-based variational method to solve this problem. Also, we implement this optimization problem based on an extremely fast approach called Bregman iteration [13, 16].

Intensity inhomogeneity is often encountered in magnetic resonance imaging (MRI) because of the bias fields [19, 20, 21]. The mathematical formulation is

$$I(\mathbf{x}) = b(\mathbf{x})J(\mathbf{x}) + n(\mathbf{x}) \tag{2}$$

at pixel $\mathbf{x}$, where I is the measured image, J is the true signal to recover, b is an unknown bias field, and n is an additive noise. The bias field is usually assumed to be spatially smooth. In Figure-2, three slices of a simulated example are shown. The goal is to recover the true signal from the given corrupted data.

(a)   (b)   (c)

(d)   (e)   (f)

(g)   (h)   (i)
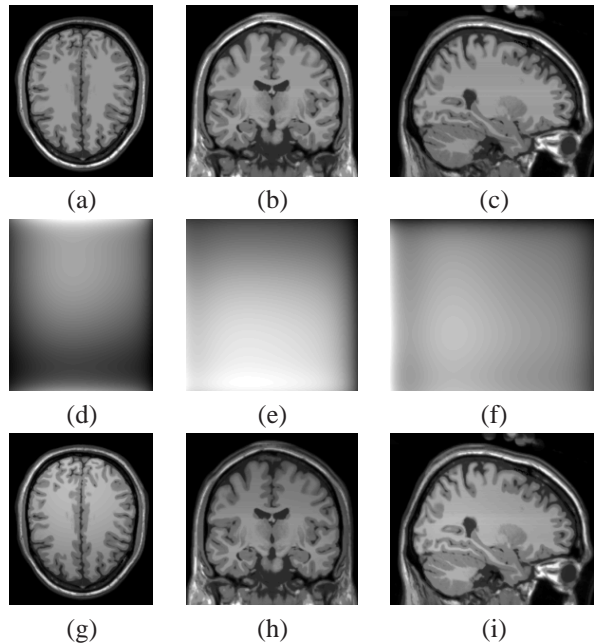
Figure 2. Simulated MRI images. (a,b,c): Clean images. (d,e,f): Bias fields simulated by polynomials. (g,h,i): Corrupted images by these fields.

There are many methods for inhomogeneity correction [20] including filtering based, surface-fitting based, segmentation based, and histogram based methods. In particular, the well-known N3 method [19] has been one of the most popular methods for inhomogeneity correction which uses B-splines to model the bias fields. It is very effective and has been used as a standard method in many medical imaging softwares. It depends on the number of node distances. Increasing the number of nodes would lead to convergence problems and increased computation time.

To simplify the formulation, as in many methods before, the noise is often ignored. Therefore, it has exactly the same form as Retinex theory. It is natural to apply Retinex algorithms to inhomogeneity correction problem. However, in MRI data, there are many small details such as vessels and tissues which are very important information for clinical diagnosis. To keep these details, we modify our original method to develop the smoothed L_1-Retinex method. We compare our algorithm with the N3 method on both simulated and real data to demonstrate the performance.

The rest of the paper is organized as follows. In section 2, we propose the mathematical formulation of our L_1-based Retinex method. In section 3, we give the implementation details. In section 4, numerical results on natural images and comparison with previous works are presented. In section 5, the smoothed L_1-Retinex method is derived for MRI images and results on both simulated and real data

are shown. Finally the conclusion and future work are discussed in section 6.

2. L_1-Retinex model

In this section, we propose a new variational model for Retinex theory. By taking a logarithm in Equation (1), we have

$$i(\mathbf{x}) = r(\mathbf{x}) + e(\mathbf{x}) \tag{3}$$

at each pixel $\mathbf{x}$, where $i = \log(I)$, $r = \log(R)$, and $e = \log(E)$. We then take the gradient:

$$\nabla i = \nabla r + \nabla e \tag{4}$$

Because of the basic assumption that the gradient of the reflectance corresponds to sharp details such as edges and the illumination is spatially smooth, ∇e is relatively small. To preserve the gradient of reflectance, a threshold function is applied to ∇i. The threshold function is defined as

$$\delta_t(\mathbf{z}) = (\tau_t(z_1), \cdots, \tau_t(z_n)) \tag{5}$$

with $\mathbf{z} = (z_1, \cdots, z_n) \in \mathbb{R}^n$, where

$$\tau_t(z) = \begin{cases} z \text{ if } |z| > t \\ 0 \text{ otherwise} \end{cases} \tag{6}$$

and the threshold t is a positive parameter. Therefore,

$$\nabla r \approx \delta_t(\nabla i) \tag{7}$$

for a suitable t.

In order to recover the true reflectance image r, a PDE-based method has been proposed by Petro Balaguer *et al.* [7, 8]. In fact, the authors of [7, 8] considered the Poisson equation

$$\Delta \hat{r} = \text{div} \delta_t(\nabla i). \tag{8}$$

which is equivalent to minimize the L_2 norm of $\nabla r - \delta_t(\nabla i)$. Suppose $\hat{r}$ is a solution to this equation, $\nabla \hat{r}$ is not necessarily equal to $\delta_t(\nabla i)$. Actually

$$\nabla \hat{r} = \delta_t(\nabla i) + \mathbf{p} \tag{9}$$

where $\mathbf{p}$ is vector field satisfying $\text{div}(\mathbf{p}) = 0$. However, $\mathbf{p}$ is usually nonsparse. This can introduce some unpredictable effects to images. For example, in a region U having constant reflectance and smoothly varying illumination, then $\text{div} \delta_t(\nabla i) = 0$ in U for a suitable threshold t. Because $\nabla \hat{r} = \mathbf{p}$ for some unknown nonsparse $\mathbf{p}$, $\hat{r}$ may not be constant in U, which is not as desired.

Another approach was proposed by Ma and Osher in [10] using a TV regularized model as follows:

$$\hat{r} = \arg\min_r \int_\Omega t|\nabla r| + \frac{1}{2}|\nabla r - \nabla i|^2 \tag{10}$$

which was implemented by Bregman iterations. And the authors in [10] showed that the first iteration is actually similar to (8), which is solving an equation

$$\Delta r_1 = \text{div shrink}_t(\nabla i) \tag{11}$$

where shrink$_t$ is an isotropic soft threshold function which is defined by

$$\text{shrink}_t(\mathbf{z}) = \begin{cases} 0 & \text{if } ||\mathbf{z}||_2 \leq t \\ \mathbf{z} - \mathbf{z}\frac{t}{||\mathbf{z}||_2} & \text{if } ||\mathbf{z}||_2 > t \end{cases} \tag{12}$$

where t is a positive parameter. The TV regularized model is efficient to recover piecewise constant images due to property of TV regularizer, but it usually loses information about reflectance.

Instead of minimizing the L_2 norm, our motivation is to minimize the L_1 norm of $\nabla r - \delta_t(\nabla i)$. Namely, our L_1-Retinex model is

$$\hat{r} = \arg\min_r \int |\nabla r - \delta_t(\nabla i)| \tag{13}$$

$$= \arg\min_r \int \sqrt{(\nabla_x r - \tau_t(\nabla_x i))^2 + (\nabla_y r - \tau_t(\nabla_y i))^2} \tag{14}$$

By minimizing the L_1 norm, we usually get a sparse vector field $\mathbf{q} = \nabla r - \delta_t(\nabla i)$. For images, if $\hat{r}$ is the solution of problem (13), then $\nabla \hat{r} = \delta_t(\nabla i)$ for most part of the domain. Thus with a high probability, we will have the reflectance $\hat{r}$ constant in the region where $\delta_t(\nabla i) = 0$.

3. Implementation

We implement the L_1-Retinex model using Bregman methods which are effective to solve sparse reconstruction problems in image processing [13]. The goal of the original Bregman method is to solve the general constrained minimization problem:

$$\min_u J(u) \text{ s.t. } H(u) = 0 \tag{15}$$

where J is convex but not necessarily differentiable, such as the L_1 norm, and H is convex and differentiable with zero as its minimum value. The original Bregman method is based on the concept of Bregman distance for a convex function J, which is given as:

$$D_J^p(u, v) = J(u) - J(v) - \langle p, u - v \rangle \tag{16}$$

where $p \in \partial J$ is a subgradient of J at the point v. Using (16), the problem (15) can be solved by Bregman iterations:

$$u^{k+1} = \arg\min_u D_J^{p^k}(u, u^k) + H(u) \tag{17}$$

$$p^{k+1} = p^k - \nabla H(u^{k+1}) \tag{18}$$

It has been proven that the sequence of u^k in the Bregman iteration converges to the solution of the constrained problem (15). The advantage of Bregman iteration is to transform a constrained problem into a sequence of unconstrained subproblems.

Our L_1-Retinex model can be effectively solved by the split Bregman method, which was introduced by Goldstein and Osher [16] for solving L_1, TV, and related regularized problems and applied to various imaging problems. The split Bregman method aims to solve the unconstrained problem:

$$\min_u J(\Phi(u)) + H(u), \tag{19}$$

where J and H are as before, and Φ is linear functional. The key idea of the split Bregman method is to introduce an auxiliary variable $d = \Phi(u)$, and try to solve the constrained problem

$$\min_{d,u} J(d) + H(u), \text{ s. t. } \frac{\lambda}{2}||d - \Phi(u)||_2^2 = 0 \tag{20}$$

where λ is a fixed positive constant. Then the original Bregman method can be applied. And u^k and d^k are updated alternatively.

For our L_1-Retinex model, we apply the split Bregman method by introducing $d = (d_x, d_y)$ as

$$d_x = \nabla_x r - \tau_t(\nabla_x i) \tag{21}$$
$$d_y = \nabla_y r - \tau_t(\nabla_y i) \tag{22}$$

then we can rewrite (13) as

$$(\hat{r}, \hat{d}) = \arg\min_{r,d} \int_\Omega \sqrt{d_x^2 + d_y^2} \text{ s.t. } d = \nabla r - \delta_t(\nabla i) \tag{23}$$

Then we can define

$$J(d, r) = \int_\Omega |d| = \int_\Omega \sqrt{d_x^2 + d_y^2}; \tag{24}$$

$$H(d, r) = \frac{1}{2}||d - \nabla r + \delta_t(\nabla i)||_2^2. \tag{25}$$

Given $r^0 = 0$ and $d^0 = b^0 = 0$, then the Bregman iterations (17) can be written as

$$(r^{k+1}, d^{k+1}) = \arg\min_{r,d} \int_\Omega |d| - \langle p_d^k, d - d^k \rangle - \langle p_r^k, r - r^k \rangle$$
$$+ \frac{\lambda}{2}||d - \nabla r + \delta_t(\nabla i)||_2^2 \tag{26}$$
$$p_d^{k+1} = p_d^k - \lambda(d^{k+1} - \nabla r^{k+1} + \delta_t(\nabla i)) \tag{27}$$
$$p_r^{k+1} = p_r^k - \lambda\text{div}(d^{k+1} - \nabla r^{k+1} + \delta_t(\nabla i)) \tag{28}$$

We assume $b^k = p_d^k/\lambda$, therefore $p_d^k = \lambda b^k$ and $p_r^k = \lambda\text{div}b^k$. Then the iterations become:

$$(r^{k+1}, d^{k+1}) = \arg\min_{r,d} \int_\Omega |d| - \lambda\langle\text{div}b^k, r\rangle - \lambda\langle b^k, d\rangle$$
$$+ \frac{\lambda}{2}||d - \nabla r + \delta_t(\nabla i)||_2^2 \tag{29}$$
$$b^{k+1} = b^k - d^{k+1} + \nabla r^{k+1} - \delta_t(\nabla i) \tag{30}$$

We then update r^k and d^k alternatively as following:

$$r^{k+1} = \arg\min_r -\lambda\langle\text{div}b^k, r\rangle + \frac{\lambda}{2}||d^k - \nabla r + \delta_t(\nabla i)||_2^2 \tag{31}$$

$$d^{k+1} = \arg\min_d \int_\Omega |d| - \lambda\langle b^k, d\rangle + \frac{\lambda}{2}||d - \nabla r^{k+1} + \delta_t(\nabla i)||_2^2 \tag{32}$$

$$b^{k+1} = b^k - d^{k+1} + \nabla r^{k+1} - \delta_t(\nabla i) \tag{33}$$

The subproblems (31) and (32) can be explicitly solved [16], which are summarized in the following algorithm.

Algorithm 1: L_1-Retinex

    input : Image i
    output: Reflectance image r

    Linearly stretch i into the range [0,255];
    Initialization: $r^0 = i$, $d^0 = 0$, $b^0 = 0$, and $k = 0$;
    while $||r^{k+1} - r^k||_2/||r^{k+1}||_2 > \epsilon$ **do**
        (i)$r^{k+1} \leftarrow \Delta^{-1}(\text{div}(\delta_t(\nabla i) + d^k - b^k))$;
        (ii)$d^{k+1} \leftarrow \text{shrink}_{\frac{1}{\lambda}}(\nabla r^{k+1} - \delta_t(\nabla i) + b^k)$;
        (iii)$b^{k+1} \leftarrow b^k - d^{k+1} + \nabla r^{k+1} - \delta_t(\nabla i)$;
        (iv)$k \leftarrow k + 1$;

    Linearly stretch r^k into the range [0,255];

In iteration (i), we update r^{k+1} by solving a Poisson equation associated with the zero Neumann boundary condition. The solution of this equation is not unique. But the difference of any two solutions is a constant. Therefore, by fixing the value of one pixel, we can get a unique solution. In practice, the equation is solved by a discrete cosine transformation (DCT). We note that the most complex part of the whole algorithm is to solve this equation. The rest of the algorithm only contains matrix multiplication and the shrink operation. Thus the whole algorithm turns to be very simple. In iteration (ii), the isotropic shrinkage function is defined in (12). It is worth mentioning that, in the first iteration, r^1 is exactly the solution to the Poisson equation (8).

4. Numerical results of L_1-Retinex

In this section, we compare our L_1-Retinex method with the PDE method in [7, 8] and the TV-Bregman method in

[10]. Theoretically, we should apply the algorithms on raw images. However, most test images are gamma-corrected. Gamma-correction means that we have already applied a concave function such as a logarithm or s^γ with $0 < \gamma < 1$ to the raw images. And all these functions have a similar shape on image domain so that the logarithm in the Retinex theory is not necessary. Therefore, all experiments in this section are done by a gamma-corrected model as suggested in [8], which means we omit the logarithm and exponent process. For the parameters, we set the convergence tolerance $\epsilon = 0.0005$ and the constant $\lambda = 1$ in the shrinkage function (12). The only parameter to be found is the threshold t.
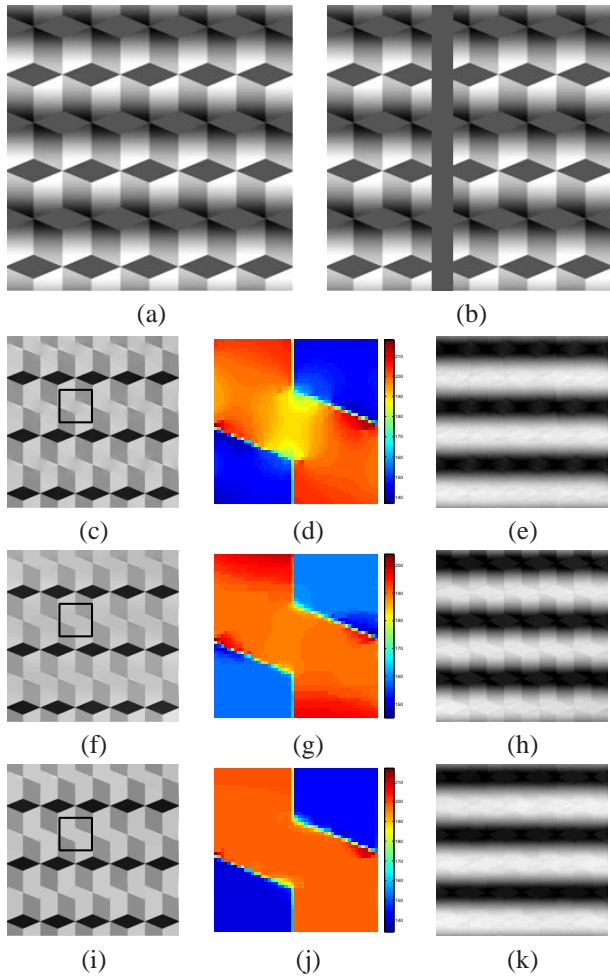
Figure 3. "Logvinenko's illusion": (a): Original image. (b): Demonstration. (c,f,i): Recovered reflectance. (d,g,j): Zoom-in version of the box in the reflectance and the color shows the intensity. (e,h,k): Recovered illumination. (c,d,e): Results from the PDE method. (f,g,h): Results from the TV-Bregman method. (i,j,k): Results from our L_1-Retinex method.

The first example is a single channel image called "Logvinenko's illusion". As shown in Figure-3, all the di-

amonds have the same intensity although we feel different. This is due to the same reason as we mentioned in "Adelson's checker shadow illusion". We set the threshold $t = 15$ for all three algorithms and the computed results are shown. The recovered reflectance images are supposed to be piecewise constant. If we zoom in the box, we can see the details which are shown in color to represent the intensity. The result from the PDE method is not piecewise constant due to the nonsparse vector field $\mathbf{p}$ as we mentioned before. The result from the TV-Bregman method is improved compared to the PDE method, but it is still not as good as the L_1-Retinex method. It should be noted that the recovered illumination image from the TV-Bregman method contains much more reflectance information than that of the other two methods. Therefore, the L_1-Retinex method gets the best result both in reflectance and illumination.
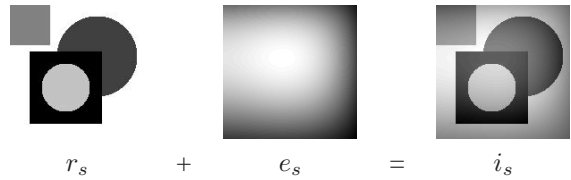
Figure 4. Simulation process

In the next example, we use a synthetic image r_s with range [0,255] as the original image. We use polynomials to simulate illumination.

$$e_s(x, y) = \sum_{i,j=0}^{3} a_{ij} x^i y^j \qquad (34)$$

where a_{ij} are random in [-1,1]. And then we rescale the range of the polynomials to [-128,128]. As in Figure-4, the simulated images i_s are the sum of a piecewise constant image r_s and the smoothed images e_s. To know the performance of different methods, we simulate 20 images. We compare the original image r_s with the recovered reflectance $\hat{r}$ from three methods with threshold $t = 20$ for PDE and L_1-Retinex and $t = 15$ for TV-Bregman. We calculate the relative distance $d(r_s, \hat{r})$ and $d(\nabla r_s, \nabla \hat{r})$ where the relative distance is defined by

$$d(\mathbf{x}, \hat{\mathbf{x}}) = \frac{||\mathbf{x} - \hat{\mathbf{x}}||_1}{||\mathbf{x}||_1} \qquad (35)$$

The results are shown in the Figure-5. In the upper figure, it is shown that the recovered reflectance from L_1-Retinex method is closer to the original image compared with the PDE method and the TV-Bregman method. In the lower figure, we can see that the gradient of reflectance from the L_1-Retinex is also closer to gradient of the original image.

The third example is a RGB image "Adelson's checker shadow illusion" shown Figure-1. We set the threshold $t =$
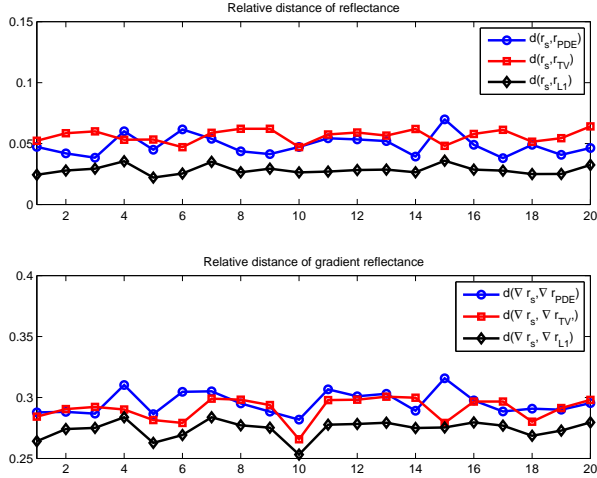
Figure 5. Top: Relative distance of reflectance. Bottom: Relative distance of gradient reflectance

12 and perform each algorithm channel by channel. We consider the pixel $P_1 = (144, 68)$ in the region A and $P_2 = (139, 111)$ in the region B, which are shown in Figure-6. The RGB value of these two pixels are shown in Table-1. The contrast of the reflectance from the L_1-Retinex method is stronger than the other two methods. The illumination image from the PDE method preserves a lot of reflectance information. The illumination image from the TV-Bregman method takes less reflectance information, but the checker and the cylinder are still visible. The illumination image from our L_1-Retinex method takes the least information of the reflectance and gives the best result.
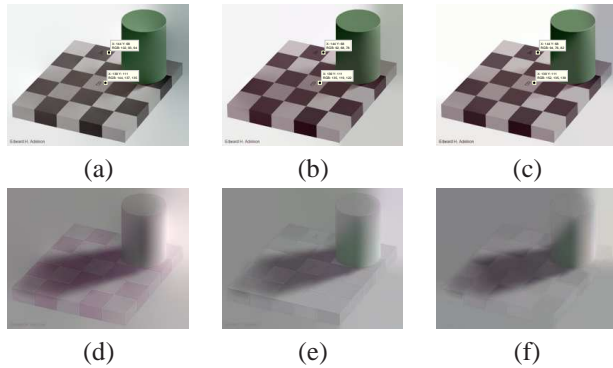
Figure 6. The result of "Adelson's checker illusion". (a,b,c): Recovered reflectance. (d,e,f): Recovered illumination. (a,d): Results from the PDE method. (b,e): Results from the TV-Bregman method. (c,f): Results from the L_1-Retinex method.

To understand the influence of the threshold t, we test on an example using HSV color space. First, we map the RGB image into the HSV space. Then the L_1-Retinex algorithm is applied to the V-channel: the intensity layer. At

RGB	PDE	TV-Bregman	L_1-Retinex
P_1	(102,93,94)	(92,68,78)	(94,76,82)
P_2	(144,137,135)	(135,119,122)	(152,135,139)

Table 1. The GRB value of the two pixels shown in Figure-6

the end, we transform it back to a RGB image only with the reflectance in the V-channel. We compare the results with different threshold t in Figure-7. The illumination (shadow effect) is eliminated gradually as t increases.
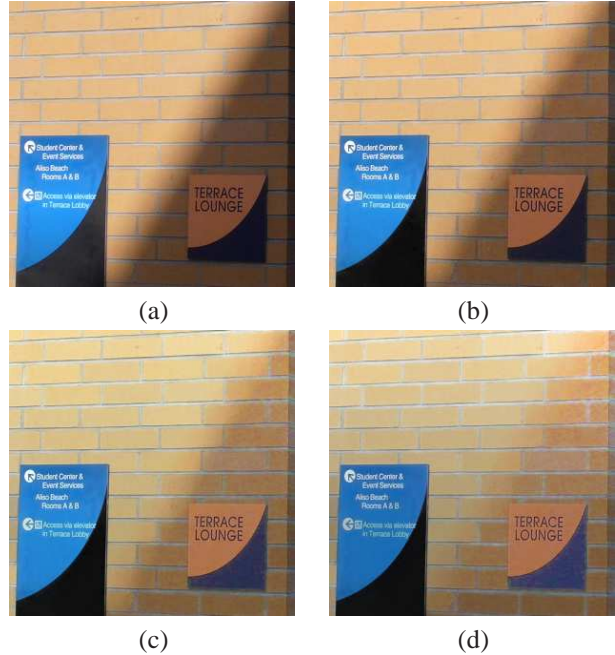
Figure 7. Influence of threshold. (a): Original image. (b): $t = 5$. (c): $t = 7.5$. (d): $t = 10$

5. Application to medical images

In medical images such as MRI, the signals sometimes are corrupted by bias fields which are similar to the natural images affected by varying illumination. Therefore, it is a good idea to apply the L_1-Retinex algorithm for solving problems in medical images. However, unlike natural images, medical images have many small details such as tissues and vessels which are very important for clinical diagnosis. So we cannot apply the L_1-Retinex method directly to medical images. Because the bias fields are spatially smooth, to take advantage of this image property, we applied the L_1-Retinex algorithm on the smoothed images which are locally averaged. When we find the illumination, the corrected image can be recovered by subtracting the illumination from the original medical image.

To find the smoothed image $\tilde{i}$, a Gaussian kernel is con-

voluted with the original image i as following

$$\tilde{i} = G_a * i \qquad (36)$$

where G_a is the Gaussian kernel with standard deviation a. Then we can apply the L_1-Retinex algorithm to $\tilde{i}$ and find the smoothed illumination $\tilde{e}$. Based on the smoothness assumption, we can suppose that $\tilde{e} \approx e$ so that the reflectance can be recovered from

$$\hat{r} = i - \tilde{e} \qquad (37)$$

The detailed algorithm is summarized as following

Algorithm 2: Smoothed L_1-Retinex

    input : Image I
    output: Reflectance image R

    1.Linearly stretch I into the range [0,255];
    2.Take logarithm: $i = \log(I + 1)$;
    3.Smooth: $\tilde{i} = G_a * i$;
    4.Apply L_1-Retinex algorithm on $\tilde{i}$ to get $\tilde{r}$;
    5.Estimate illumination: $\tilde{e} = \tilde{i} - \tilde{r}$;
    6.Extract reflectance: $\hat{r} = i - \tilde{e}$;
    7.Linearly stretch $\hat{r}$ into the range $[0, \log(255)]$;
    8.Take exponent: $\hat{R} = \exp(\hat{r})$;

We apply the smoothed L_1-Retinex method on both simulated and real data and and compare the results with that of the N3 method [19] which is one of the most popular methods in inhomogeneity correction. Our method can be directly extended to 3D. For now we only test it in the 2D case.

A clean MRI brain image from BrainWeb [1] is used as simulated data, and three slices are chosen as test images. As in [21], we use polynomials with random coefficients to simulate bias fields as in Equations (34). The bias fields are scaled to [0.5,1.5] and then multiply the clean images. Figure-2 are three examples. We compare our smoothed L_1-Retinex algorithm with the N3 method [19]. In the proposed method, the parameters are set as the threshold $t = 1.5$, the standard deviation $a = 1$, the discrete Gaussian kernel a 25 by 25 matrix, and the convergence tolerance $\epsilon = 0.0005$. We use MIPAV[2] [22] for the N3 algorithm. The parameters are set as signal threshold 1, convergence tolerance 0.001, Field distance 60.333, max number of iteration 500, subsampling 1.0, Kernel fwhm 0.15, and Wiener filter noise 0.001. Results of test images in the bottom row of Figure-2 are shown in Figure-8. We find that the visual quality of result images are similar by these two methods.
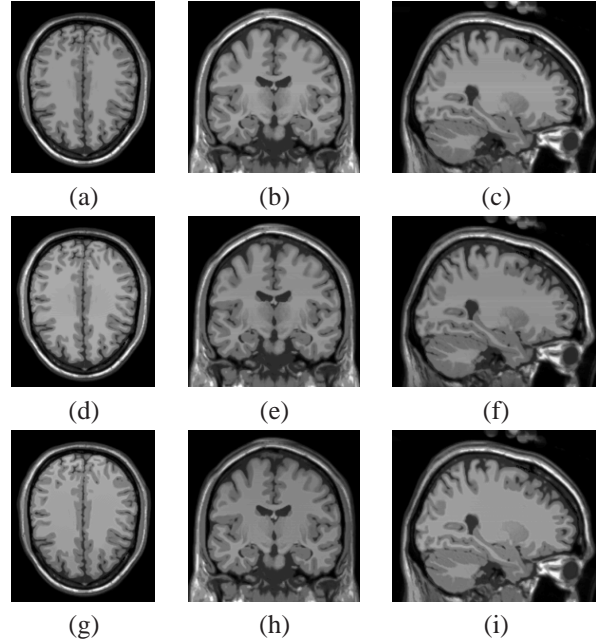
Figure 8. Results of simulated MRI images. (a,b,c): Clean data. (d,e,f): N3 corrected images. (g,h,i): recovered images by the smoothed L_1-Retinex method.

We also apply our method to a set of real clinical MRI data as shown in Figure-9. From left to right are two sagittal images and one coronal image of the head and neck MRI from the same patient. In the original clinical images (Figure-9 top row), there is apparent bias field effect at the neck area. The middle row of Figure-9 are the results of the N3 method using the same software in previous paragraph. The parameters are set as signal threshold 1, convergence tolerance 0.001, Field distance 83.333, max number of iteration 500, subsampling 1.0, Kernel fwhm 0.15, and Wiener filter noise 0.001. The bottom row of Figure-9 are the results from the smoothed L_1-Retinex with parameters $t = 2$, $a = 5$, and $\epsilon = 0.0005$, and discrete Gaussian a 25 by 25 matrix. In the original image, we can hardly observe the area of the neck due to bias fields. Improved images obtained by both N3 and smoothed L_1-Retinex. However, the details near the lower neck area are significantly visible by the smoothed L_1-Retinex method.

6. Conclusion

We propose a new method for Retinex theory, which is effective in recovering reflectance from natural images. Our method is based on minimizing an L_1 norm, which ensures that both the recovered reflectance and illumination have better quality than previous works. Examples and statistics are shown in the paper to demonstrate the performance of our method. Besides, this algorithm can be applied to shadow elimination problem and image enhancement.
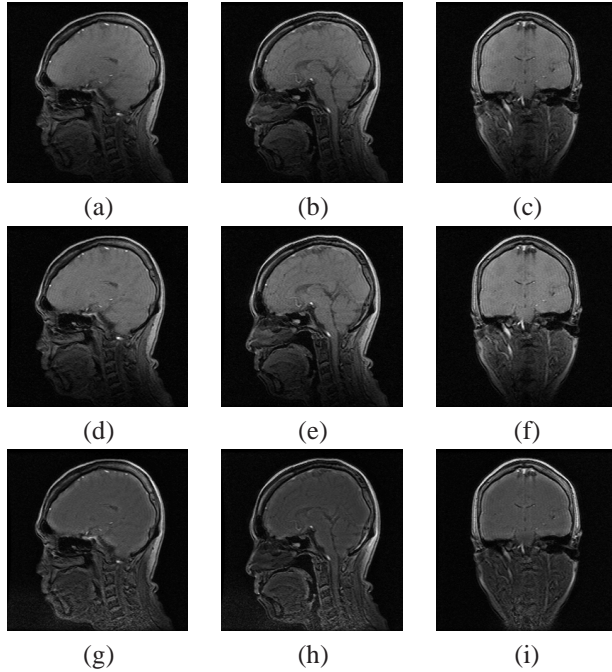
Figure 9. Real data: (a,b,c): Original. (d,e,f): N3 corrected images. (g,h,i): Corrected images by the smoothed L_1-Retinex method.

A modified method is developed for inhomogeneity correction problem for MRI data. Both simulated and real data are tested. From the clinical example, we show that our method can substantially increase the visual quality.

We can easily extend the method to 3D for medical image reconstruction. Our method can be applied to other data such as hyperspectral images. The method itself can be modified by adding a regularizer based on the properties of images. All of these will be in our future work.

Acknowledgements

References

[1] E. H. Land, J.J. McCann. Lightness and the Retinex theory. *J. Opt. Soc. Am.*, 61(1):1-11, 1971.

[2] E. H. Land. The Retinex theory of color vision. *Sci. Amer.*,237(6):108-128, 1977.

[3] E. H. Land. Recent advances in Retinex theory and some implications for cortical computations: Color vision and the natural image. *Proc. Nat. Acad. Sci. USA*, 80:5163-5169, 1983.

[4] E. H. Land. An alternative technique for computation of the designator in the Retinex of color vision. *Proc. Nat. Acad. Sci. USA*, 83:3078-3080, 1986.

[5] A. Blake. Boundary conditions of lightness computation in mondrian world. *Computer Vision Graphics and Image Processing*, 32:314-327, 1985.

[6] B. K. P. Horn. Determining lightness from an image. *Computer Graphics and Image Processing*, 3:277-299, 1974.

[7] J. M. Morel, A. B. Petro, and C. Sbert. Fast implementation of color constancy algorithms. *Proc. SPIE*, 7241, 724106, 2009. DOI:10.1117/12.805474

[8] J. M. Morel, A. B. Petro and C. Sbert. A PDE Formalization of Retinex Theory. *IEEE Trans. on Image Processing*, 19(11):2825-2837, 2010.

[9] R. Kimmel, M. Elad, D. Shaked, R. Keshet, and I. Sobel. A variational framework for Retinex. *Int. Journal of Computer Vision*, 52(1):7-23, 2003.

[10] W. Ma, S. Osher, A TV Bregman iterative model of Retinex theory. *UCLA CAM Report* 10-13, 2010.

[11] Y. Lei, Y. Zhou, J. Li. An Investigation of Retinex algorithms for image enhancement. *Jouranl of Electron (China)*, 24(5):696-700, 2007.

[12] D. Brainard, B. Wandell. Analysis of the Retinex theory of color vision. *J. Opt. Soc. of Am. A*, 3(10):1651-1661, 1986.

[13] S. Osher, M. Burger, D. Goldfarb, J. Xu, and W. Yin. An iterative regularization method for total variation based image restoration. *SIAM Multiscale Model. and Simu*, 4:460-489, 2005.

[14] J. Frankle, J. McCann. Method and apparatus for lightness imaging. US Patent no. 4384336, 1983.

[15] B. Funt, F. Ciuera, J. McCann. Retinex in Matlab. *Journal of Electronic Imaging*, 13(1):48-57, 2004.

[16] T. Goldstein and S. Osher. The split Bregman algorithm for L1 regularized problems. *SIAM J. Imaging Sci.*, 2(2), 323-343, 2009.

[17] D. J. Jobson, Z. Rahman, G. A. Woodell. A multiscale Retinex for bridging the gap between color images and the human observation of scenes. *IEEE Trans. on Image Processing*, 6(7):965-976, 1997.

[18] E. Provenzi, M. Fierro, A. Rizzi, L. D. Carli, D. Gadia, and D. Marini. Random spray Retinex: A new Retinex implementation to investigate the local properties of the model. *IEEE Transactions on Image Processing*, 16(1):162-171, 2007.

[19] J. G. Sled, A. P. Zijdenbos, A. C. Evans. A nonparametric method for automatic correction of intensity nonuniformity in MRI data. *IEEE Transactions on Medical Imaging*, 17(1):87-97, 1998.

[20] U. Vovk, F. Pernus, and B. Likar. A review of methods for correction of intensity inhomogeneity in MRI. *IEEE Trans. on Medical Imaging*, 26(3):45-421, 2007.

[21] Y. Zheng, J. C. Gee. Estimation of Images Bias Field with Sparsity Constraints. *IEEE Computer Vision and Pattern Recognition (CVPR)*, 2010.

[22] Medical Image Processing, Analysis and Visualization. Version 5.5.1, Center for Information Technology, National Institues of Health.